Tropospheric sulfate from Cumbre Vieja volcano at Las Palmas, transported towards Cabo Verde - lidar measurements of aerosol extinction, backscatter and depolarization at 355, 532 and 1064 nm

Henriette Gebauer[1,2], Athena Augusta Floutsi[1], Moritz Haarig[1], Martin Radenz[1], Ronny Engelmann[1], Dietrich Althausen[1], Annett Skupin[1], Albert Ansmann[1], Cordula Zenk[3,4], and Holger Baars[1]

[1]Leibniz Institute for Tropospheric Research, Leipzig, Germany
[2]Institute for Meteorology, Leipzig University, Leipzig, Germany
[3]Ocean Science Center Mindelo, Mindelo, Cabo Verde
[4]GEOMAR Helmholtz Centre for Ocean Research, Kiel, Germany

Correspondence: Henriette Gebauer (gebauer@tropos.de)

Abstract. From 19 September to 13 December 2021, volcanic eruptions took place at the Cumbre Vieja ridge, Las Palmas, Canary Islands. Thereby, fine ash and volatiles, like sulfur dioxide (SO_2), were emitted and transported over hundreds to thousands of kilometers away from the island. Continuous lidar observations with the multiwavelength-Raman-polarization lidar Polly^{XT} were performed at the Ocean Science Center at Mindelo, Cabo Verde, in the framework of the Joint Aeolus-Tropical Atlantic Campaign (JATAC) 2021/2022 enabling the characterization of the atmospheric state above Mindelo during the eruption period. A special feature of the system operated at Mindelo is, that measurements of the particle extinction coefficient, the particle extinction-to-backscatter ratio (lidar ratio) and the particle linear depolarization ratio are available at all three wavelengths (355, 532 and 1064 nm). The typical aerosol conditions over Mindelo are a clean marine planetary boundary layer (PBL) up to approx. 1 km and above a Saharan dust layer (SAL, up to 6 km) during northern hemispheric summer and fall. A particle extinction coefficient smaller than $200 \, \mathrm{Mm}^{-1}$, a lidar ratio smaller than 30 sr and a particle linear depolarization ratio close to 0 % have been typically observed within the planetary boundary layer, while a lidar ratio between 40 and 60 sr and a linear depolarization ratio between 20 and 30 % are characteristic for the SAL above. In contrast, during the time of the volcanic eruptions, a strongly polluted PBL was observed on specific days beginning on the 23 September 2021, whereby the particle extinction coefficient and the lidar ratio increased up to $800 \, \mathrm{Mm}^{-1}$ and 80 sr (at 355 nm), respectively. On 24 September, the aerosol optical depth, determined by an AERONET (Aerosol Robotic Network) sun photometer, was as high as 0.9 and 1.1 (daily averages at 500 and 340 nm). HYSPLIT (Hybrid Single-Particle Lagrangian Integrated Trajectory) trajectories indicate air mass transport from Canary Islands to Mindelo at heights below 2 km. The observed pollution in the PBL over Mindelo is attributed to sulfate aerosol from the volcanic eruption at Las Palmas as the particle linear depolarization ratio was low (≤ 3 %) and, thus, does not indicate non-spherical particles, such as Saharan dust or volcanic ash. We thus conclude that sulfate aerosol formed from gaseous precursors during the transport (2–3 days for a distance of 1500 km) from Las Palmas towards Cabo Verde. No indications of volcanic ash over Mindelo were found in the SAL. This finding is supported by the HYSPLIT

trajectories, which show that air masses in higher altitudes originate from the African continent and not from the Canary Islands.

1 Introduction

25 Volcanic eruptions are of large importance for the Earth's climate (Hansen et al., 1997; Robock, 2000) because the emitted particles and gases can be transported several hundreds of kilometers away from the source and influence the global radiation budget (Solomon et al., 2011; Groß et al., 2012; Martin et al., 2014). Typically emitted products of volcanic activity are ash particles with a diameter lower than 2 mm during explosive phases, as well as volatiles such as sulfur dioxide (SO_2; McGonigle et al., 2004; Aiuppa et al., 2008; Carracedo et al., 2022). SO_2 is the most abundant gas emitted by volcanoes (Kampouri et al.,

30 2021) of which 10–20 Mt are released into the troposphere each year (Martin et al., 2014). While in the stratosphere this gas has a lifetime of multiple weeks, it persists in the troposphere for around 1–3 days (Navas-Guzmán et al., 2013; Pattantyus et al., 2018). In a chemical reaction with water and further atmospheric components (hydroxyl radical (OH) in clear air conditions or hydrogen peroxide (H_2O_2) in cloudy air) it is quickly converted to sulfate aerosol (SO_4^{2-} bearing substances and sulfuric acid droplets; Ansmann et al., 2011b; Martin et al., 2014; Pattantyus et al., 2018). The efficiency of the conversion of SO_2 to

35 sulfate aerosol is influenced by multiple factors and increases with temperature and relative humidity (Eatough et al., 1994; Yang et al., 2018). The lifetime of sulfate aerosol in the troposphere of 1 to 3 weeks is much longer than the one of SO_2 or volcanic ash, so that it can be transported over long distances (Pappalardo et al., 2004; Filonchyk et al., 2022). If it reaches the higher troposphere/lower stratosphere it can remain even for several years (Jäger, 2005; Deshler, 2008; Martin et al., 2014).

Sulfate aerosol particles have several climate impacts since they reflect solar radiation (Pappalardo et al., 2004) and scatter

40 light even more efficiently with increasing relative humidity due to hygroscopic growth (Miffre et al., 2012). Furthermore, they act as cloud condensation nuclei (CCN) and ice nucleation particles (INPs) and, thus, influence the precipitation cycle (Pappalardo et al., 2004). Especially in cities, sulfate aerosol is of large importance with regard to air quality. It is one of the major components of urban PM2.5 (Zhang et al., 2004; Yang et al., 2018). Although anthropogenic SO_2 emissions are with 110 Mt per year 5–10 times higher than volcanic emissions, volcanic eruptions are one of the greatest natural sources for

45 sulfur emissions (Martin et al., 2014). Furthermore, their emissions have a larger climate impact due to the release of SO_2 in higher altitudes, which provides a longer lifetime of the formed aerosol particles (Kampouri et al., 2021). In addition, sulfate particles can be emitted directly as well (Martin et al., 2014). Moreover, volcanic eruptions have not only climatological but also economical impact with regard to aviation. For example, volcanic ash can cause engine damage at aircraft or air traffic is even suspended, as happened during the eruption of the Iceland volcano Eyjafjallajökull in spring 2010 (Groß et al.,

50 2012). To reduce the risks, ash-dispersion simulations are used in early warning systems. Assimilation of satellite products like Aeolus wind measurements improve the ash plume forecast, as shown in a recent study of Amiridis et al. (2023). Besides the climatological and economical consequences, volcanic gases and particles regionally lead to strong pollution events, too, in fact during volcanic eruptions villages in the proximity even have to be evacuated. Often, the visibility is reduced and extremely unfavorable air quality is caused (Pattantyus et al., 2018). As a dominant component of PM2.5, sulfate aerosol has a negative

55 impact on human health as it infiltrates deeply into the lung and can cause asthma, sinusitis or further respiratory disease (Businger et al., 2015).

Lidar observations have expanded our knowledge on volcanic aerosol in the troposphere. In the case of the eruption of Eyjafjallajökull in Iceland in 2010 (Ansmann et al., 2010, 2011b; Groß et al., 2012; Pappalardo et al., 2013) and Etna in Italy in 2002 (Pappalardo et al., 2004) and 2019 (Kampouri et al., 2021) pure volcanic ash was observed. Lidar ratios in the
60 range of 30–60 sr and a particle linear depolarization ratio of 35–37 % were measured at 355 and 532 nm. In general, it is challenging to distinguish volcanic ash from other depolarizing aerosol types, especially from desert dust, because of the very similar lidar ratios of both types. The main quantity for the distinction between volcanic ash and desert dust is the particle linear depolarization ratio, which is in the range of 30±5 % for pure dust (Ansmann et al., 2010) and, thus, smaller than the aforementioned values for ash. Sulfate aerosol instead can be distinguished more easily from volcanic ash due to a much
65 lower particle linear depolarization ratio and the different size ranges of the aerosol particles (fine mode (diameter $\leq 2\,\mu m$) for sulfate aerosol and coarse mode (diameter $> 2\,\mu m$) for volcanic ash; John et al., 2011). A separation of volcanic sulfate and ash based on the particle linear depolarization ratio was successfully introduced by Ansmann et al. (2011b). Sulfate particles produce a larger lidar ratio (55 up to 80 sr) and a particle linear depolarization ratio close to zero (4–5 %) as multiwavelength-Raman lidar observations at 355 and 532 nm during the eruptions of Eyjafjallajökull and Etna have shown. In the case of
70 Eyjafjallajökull, Navas-Guzmán et al. (2013) observed two distinct aerosol layers over Granada, Spain, consisting to 82 % of sulfate aerosol. Sulfate aerosol from Eyjafjallajökull mixed with continental aerosol was furthermore observed in the planetary boundary layer (PBL) over Potenza, Italy, (Mona et al., 2012). One of the first multiwavelenth-Raman lidar observations of tropospheric volcanic aerosol, and especially sulfate particles (mixed with a low amount of soot), was also performed at Potenza by Pappalardo et al. (2004) capturing the eruption of Etna in 2002.

75 One of the most recent volcanic eruptions, which was highly present in the European media, took place at the Cumbre Vieja volcanic ridge (28.34°N, 17.50°E, 1949 m a.s.l. (Filonchyk et al., 2022)) at Las Palmas, Canary Islands. The event is described in detail by Carracedo et al. (2022). Further studies concerning its impact on air quality were performed by Filonchyk et al. (2022) and Milford et al. (2023). Volcanic activity started on 19 September 2021. The last eruption was recorded on 13 December 2021. The volcanic activity during this period was classified as a basaltic fissure eruption dominated by strombolian
80 activity and with episodic phreatomagmatic pulses. The eruptive column usually reached to an altitude of 3500 m a.s.l. and peaked at 8500 m a.s.l. on 13 December. During the whole time of volcanic activity, fine lapilli (diameter 2–64 mm) were constantly produced. In addition, ash (<2 mm) and more than 10 kt SO_2 per day were emitted (Filonchyk et al., 2022) so that locally the European air quality hourly threshold of $350\,\mu gm^{-3}$ was exceeded on multiple days (Milford et al., 2023). The SO_2 emissions were largest at the beginning of the period with a maximum of 125 kt on 23 September 2021 (Milford et al., 2023).
85 According to SO_2-dispersion forecasts (Carracedo et al., 2022), the emission products were transported over long distances reaching Central Europe and the Caribbean.

Volcanic aerosol of this eruption was also transported towards Mindelo on the Cabo Verdean Islands, which are located 1500 km southwest of the Canary Islands. Since June 2021, the multiwavelength-Raman-polarization lidar Polly^{XT} (Engelmann et al., 2016; Baars et al., 2016), has been operated there and was able to observe the volcanic aerosol. On specific days, the

90 volcanic particles caused a high aerosol optical depth (AOD) around 1.0 and a strong pollution in the PBL with extinction
coefficient values more than twice as much as the typical background conditions and a highly reduced visibility. Since Cabo
Verde is located in the trade wind zone with preferred direction of inflow from north east, i.e., from Canary Islands, we will
show that the volcanic aerosol reached the measurement site at a low altitude and, thus, had a significant relevance with regard
to air quality and human health impacts.

95   In this paper, we present a case study of lidar observations conducted on the 24 September 2021 (period of volcanic activity)
at Mindelo, Cabo Verde. The lidar observations indicate a strong pollution by volcanic sulfate aerosol. In the following section,
the methodology is described, including information about the instruments and models, the measurement site and the way of
data processing. In Sect. 3, the results for the case study are presented and discussed in Sect. 4, before a conclusion is drawn in
Sect. 5.

100 2   Methodology

2.1   Measurement site and instrumentation

In the frame of the ground-based part (ASKOS) of the Joint Aeolus-Tropical Atlantic Campaign (JATAC) (Amiridis et al.,
2022; Fehr et al., 2023; Marinou et al., 2023), a temporary ACTRIS (Aerosol, Clouds and Trace Gases Research Infrastructure)
station was set up at the Ocean Science Center Mindelo (OSCM) at Mindelo, Cabo Verde, (16.878°N, 24.995°E) in June 2021.
105 The OSCM is located on the west coast of the island of Ŝao Vicente, so that the anthropogenic influence is low. The island
itself is located 1500 km southwest of the Canary Islands and Las Palmas and in the trade wind zone with usual advection of
air masses from north easterly direction. Typically, cumulus convection occurs at Mindelo during nighttime.

Amongst others, this station is equipped with a Polly$^{\text{XT}}$ multiwavelength-Raman-polarization lidar. The lidar deployed at
Mindelo has a few improvements, compared to previous instruments (Althausen et al., 2009; Engelmann et al., 2016). For
110 instance, it uses a diode pumped laser, which has a higher repetition rate (100 Hz) than the typical Nd:YAG laser (20–30 Hz)
of Polly$^{\text{XT}}$. This feature offers the possibility to retrieve profiles of the optical properties with a lower temporal averaging
down to 10 min. It is an important capability with regard to this study, since at Mindelo often small clouds occur during night
and cloud-free periods are quite short. Furthermore, the receiver consists of 15 channels and enables measurements of the
elastic backscatter coefficient at 355, 532 and 1064 nm, the inelastic backscatter at 387, 607 and 1058 nm, the cross-polar
115 signal at 355, 532 and 1064 nm and the inelastic signal from water vapour at 407 nm. Additionally, near-field measurements are
available for the 355 and 532 nm elastic channels and the 387 and 607 nm Raman channels. The instrument has also a dual-field-
of-view depolarization channel (Jimenez et al., 2020). With this setup, aerosol optical quantities can be determined. These are
the particle backscatter coefficient, the particle extinction coefficient, the lidar ratio (ratio of particle extinction-to-backscatter
coefficient) and the particle linear depolarization ratio, all at 355, 532 and 1064 nm, as well as the backscatter-related Ångström
120 exponent between the different wavelengths and the extinction-related Ångström exponent. The availability of the extinction
coefficient, the lidar ratio and the particle linear depolarization ratio at 1064 nm as well as the backscatter coefficient at this
wavelength determined via the rotational-Raman (RR) channel is a new feature of this device. A liquid cloud base on 4

October 2021 was used to estimate the cross talk of the elastic signal in the rotational Raman signal at 1058 nm (Haarig et al., 2016, 2022). As every Polly^{XT} lidar system, the Polly^{XT} lidar that operates at Mindelo is part of Polly^{NET} (Baars et al., 2016) and vertical profiles of the lidar optical properties are automatically derived by the Polly^{NET} processing chain (Yin and Baars, 2021). However for this study, the profiles were analyzed manually. Due to the frequent occurrence of boundary layer clouds a more tailored data analysis was needed. Otherwise optical profiles were not derived by the automatic processing chain having a strict cloud screening and other quality control measures.

In addition, a CIMEL Sun Sky Lunar photometer of type CE318-T was used for this study, which is operating in the Aerosol Robotic Network (AERONET Holben et al., 1998). It measures solar irradiances at 8 different wavelengths (340, 380, 440, 500, 675, 870, 1020 and 1640 nm) from which the AOD (at the same wavelengths), the columnar Ångström exponent (for 6 wavelength pairs), the volume size distribution, the refractive index, the single scattering albedo, the absorption AOD, the extinction AOD, the asymmetry factor, and the phase function are derived. A new capability of the latest type CE318-T is that it measures during night as well using the moonlight to determine nighttime AODs.

2.2 Air mass source attribution

To describe the origin of the observed air masses, Hybrid Single-Particle Lagrangian Integrated Trajectories (Stein et al., 2015; Rolph et al., 2017; HYSPLIT, 2023) were used. Ensemble trajectories with 27 members were calculated for 5 days back in time, i.e., towards the day when volcanic activity at Las Palmas started. The meteorological input data was taken from the Global Data and Assimilation Service (GDAS1, 2023). Furthermore, simulations with the Lagrangian dispersion model FLEXPART (Radenz et al., 2021) were performed using meteorological data fields from the Global Forecast System (GFS; National Centers for Environmental Prediction, National Weather Service, NOAA, U.S. Department of Commerce, 2000). In this case, 5-day backward simulations were calculated for 500 air parcels which arrive at Mindelo at different altitudes from 0 to 10 km in steps of 500 m with a temporal resolution of 3 h. Evaluating both backward simulation models allow us to ensure more certainty with respect to the origin of the air masses.

In addition, the distribution of the volcanic plume was monitored. Therefore, the transport of SO_2 and its advection towards Mindelo was tracked. For this purpose, the TROPOspheric Monitoring Instrument (Veefkind et al., 2012; TROPOMI, 2023) on board the polar orbiting Sentinel-5 Percursor satellite can be used, which offers daily global measurements of the amount of SO_2 molecules in a column per surface area. Its horizontal resolution is $3.5 \times 5.5 \, \text{km}^2$.

3 Results

A time series of the AOD at different wavelengths and the columnar Ångström exponent between 440 and 870 nm is shown in Fig. 1. Before the start of the eruption, the hourly mean AOD was about 0.4. Hourly mean Ångström exponent values of 0.2 were usually observed until 22 September. During the time of volcanic activity, a change in the behaviour of the Ångström exponent and the AOD could be seen since 22 September and thus 3 days after the eruption started. A strong increase of the Ångström exponent to values higher than 0.8 was measured. In that time, high AODs, with values close to 1.0, were recorded,
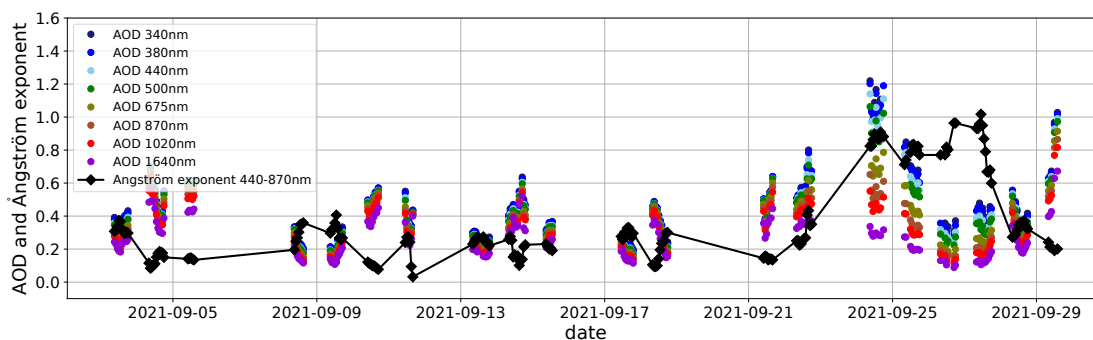
Figure 1. Time series of Level 2.0 hourly averages of the aerosol optical depth (AOD) at different wavelengths and the columnar Ångström exponent between 440 and 870 nm measured with an AERONET sun photometer at Mindelo in September 2021. Data points for the 16 September were cut out, since on that day a cirrus was present, which was not correctly screened out by the AERONET retrieval. The original data, including the cirrus, is added in the Appendix (Fig. A1). The data was taken from AERONET (2023).

155 e.g., on 24 and 29 September 2021. On 24 September, the daily mean AOD was 1.1 at 340 nm and 0.9 at 500 nm. The vertically-resolved lidar optical properties are presented in a case study for 24 September (Sect. 3.2) contrasted to background conditions before the volcanic eruption (16 September, Sect. 3.1), representing a clean planetary boundary layer (marine influenced).

3.1 Reference case (16 September 2021)

To contrast the differences between the volcanic influenced aerosol conditions over Mindelo and the typical situation before
160 the start of the eruption at Las Palmas, the 16 September 2021 was selected as reference observation. The corresponding height-resolved temporal development of the attenuated backscatter coefficient at 1064 nm and the volume depolarization ratio at 532 nm is shown in Fig. 2 (left side). During that day, two different aerosol layers were present. The planetary boundary layer reached up to 0.8 km height. In that layer, no depolarization occurred (Fig. 2b). Above, a lofted layer, which was strongly depolarizing, was located between 1.2 and 6 km height. Small clouds were frequently present in the PBL. They can be identified
165 in Fig. 2a as red spots above which stripes of missing signal are visible. This layering has been typically observed over Mindelo from June to October 2021 and is in agreement with previous studies on this archipelo (Ansmann et al., 2011a; Groß et al., 2011; Rittmeister et al., 2017). Additionally, on the reference day a cirrus occurred, which was not correctly screened out by the AERONET algorithm (cf. Fig. A1 and Fig. A2). Thus, there are no usable sun photometer data for the 16 September.

Vertical profiles of the lidar optical properties (Fig. 3) were derived with the Raman method (Ansmann et al., 1992) for a
170 48-min interval in the evening (22:24–23:12 UTC, red rectangle in Fig. 2, left side), since this was the longest cloud-free period during nighttime. The corresponding mean values are summarized in Table 1. In the lofted layer, the mean lidar ratio between 1.3 and 5.3 km of 58.4 and 47.3 sr (at 355 and 532 nm) and the particle linear depolarization ratio of 24.5, 28.1 and 24.1 % (at 355, 532 and 1064 nm) are in a typical range for desert dust (Haarig et al., 2017; Floutsi et al., 2023). In the PBL, relatively clean marine conditions (Bohlmann et al., 2018) were observed, which were characterized by a mean lidar ratio of 17.4 and
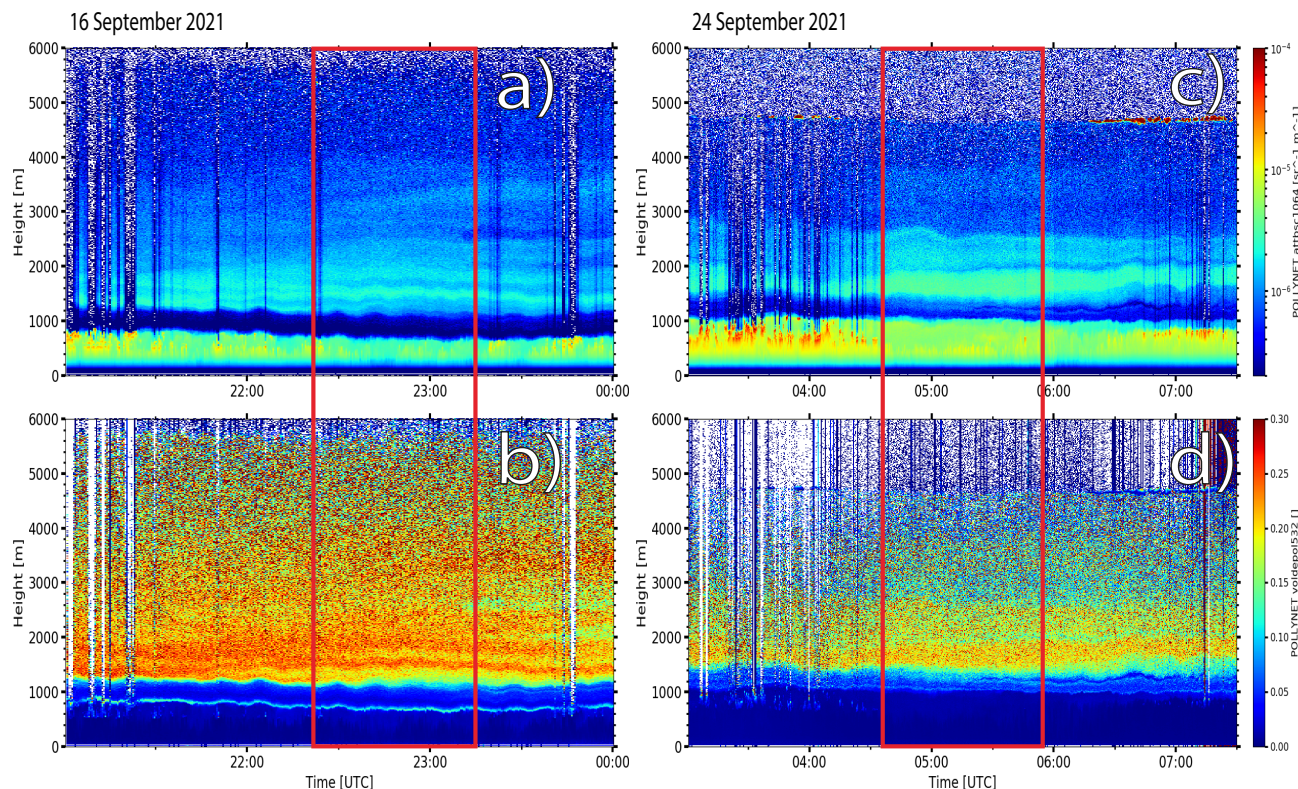
Figure 2. Temporal evolution of the height-resolved attenuated backscatter coefficient at 1064 nm (top) and the volume depolarization ratio at 532 nm (bottom) measured by Polly^{XT} at Mindelo, Cabo Verde, during 16 September 2021, 21:00–24:00 UTC, (left) and 24 September 2021, 03:00–07:30, (right).

175   23.7 sr (at 355 and 532 nm) between 0.25 and 0.6 km and a mean particle linear depolarization ratio of 0.7, 1.1 and 1.0 % (at 355, 532 and 1064 nm) between 0.06 and 0.6 km. The mean particle extinction coefficient was about 114 and 130 Mm^{-1} (at 355 and 532 nm) between 0.25 and 0.6 km. Unfortunately, for that day the rotational-Raman profiles at 1064 nm were not available since the analyzed time period of 48-min is too short to obtain reasonable results. However, the measurement from the 16 September represents the typical values, which we usually observed over Mindelo during that time of the year. This statement

180   is valid especially for the PBL.

3.2   Volcanic influence

For the the 24 September 2021, the height-resolved temporal development of the attenuated backscatter coefficient at 1064 nm is shown in Fig. 2c and the volume depolarization ratio at 532 nm in Fig. 2d. Again, two distinct aerosol layers are visible – a very low depolarizing PBL (Fig. 2d) up to about 1 km height and a strongly depolarizing lofted layer from 1.4 to 5 km height.
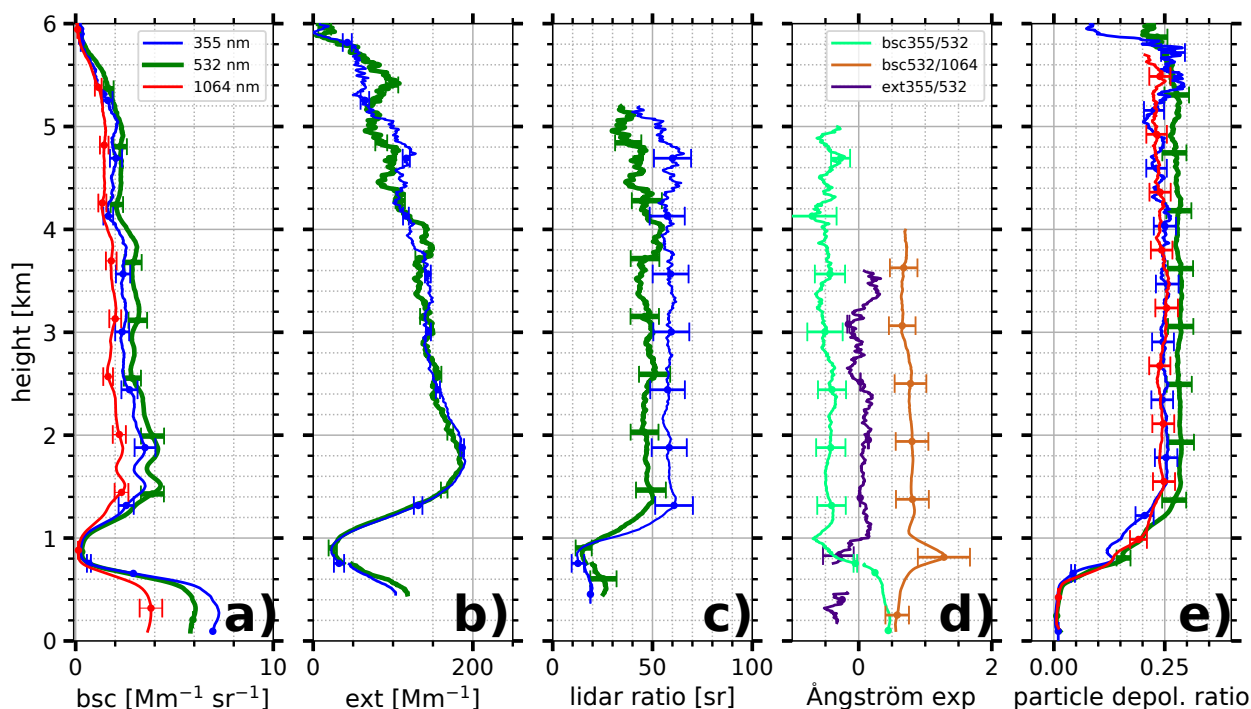
Figure 3. Measured with Polly[XT] at Mindelo, Cabo Verde, on 16 September 2021, between 22:24 and 23:12 UTC: vertical profiles of (a) the particle backscatter coefficient, (b) the particle extinction coefficient, (c) the lidar ratio, (d) the Ångström exponent and (e) the particle linear depolarization ratio. Backscatter and depolarization profiles as well as the backscatter-related Ångström exponent are plotted with a vertical smoothing of 187.5 m. The vertical smoothing for the remaining quantities is 742.5 m. Near- and far-field measurements are merged at 750 m.

185   As on 16 September, often small clouds occurred in the PBL. Before first daylight appeared at 07:30 UTC, a longer cloud free period evolved. Thus, optical properties were retrieved with the Raman method for an 1:19 h interval (04:38–05:57 UTC, indicated by a red rectangle in Fig. 2, right side).

     The corresponding vertical profiles are shown in Fig. 4. On that day, all lidar-derived optical quantities are available at all three wavelengths. For the lofted layer, mean values, as depicted in Table 1, were retrieved based on the far-field measurements

190   considering a vertical extent of 1.4–4.4 km and a vertical smoothing as in Fig. 4. The particle backscatter coefficient varied from $0.8 \, \mathrm{Mm^{-1} sr^{-1}}$ (minimum at 355 nm) to $5.0 \, \mathrm{Mm^{-1} sr^{-1}}$ (maximum at 532 nm) and the particle extinction coefficient from $16 \, \mathrm{Mm^{-1}}$ (minimum at 532 nm) to $246 \, \mathrm{Mm^{-1}}$ (maximum at 532 nm). Measurements of the lidar ratio led to layer mean values of 65.3, 50.7 and 68.7 sr (355, 532, and 1064 nm, respectively). These values are slightly larger than the once measured on 16 September, which were similar compared to previous observations of pure Saharan dust (50–60 sr at 355 and 532 nm;
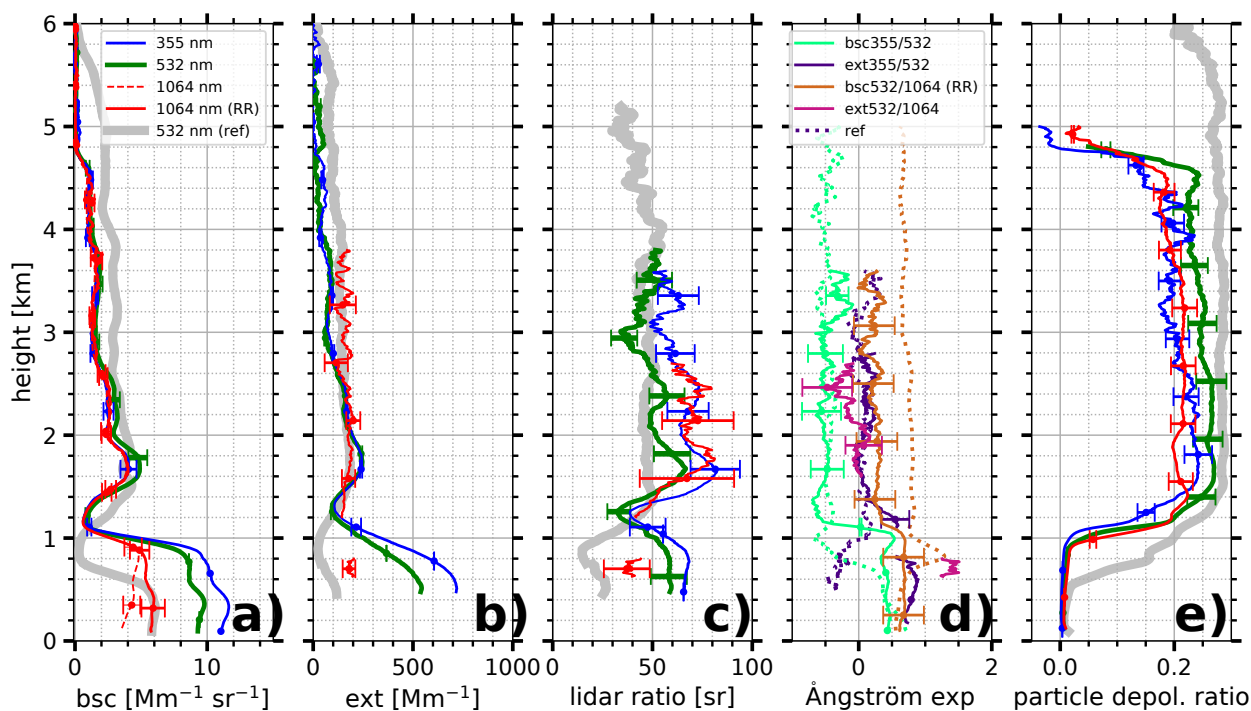
Figure 4. Same as in Fig. 3 but for the 24 September 2021, between 04:38 and 05:57 UTC. For that day, profiles of the particle extinction coefficient and the lidar ratio are available at 1064 nm, too, as well as the extinction-related Ångström exponent between 532 and 1064 nm. For them, the vertical smoothing is 397.5 m (below 1.2 km) and 1492.5 m (above 1.2 km). Near- and far-field measurements are merged at 1100 m. Additionally, the reference profiles from 16 September 2021 at 532 nm (thick grey line and dotted lines for the Ångström exponent and labelled as "ref") are shown, representing the typical aerosol conditions over Mindelo with a clean marine PBL.

195   Ansmann et al., 2011a; Groß et al., 2011; Floutsi et al., 2023) The lidar ratio at 1064 nm is in line with dust observations at Leipzig, Germany (Haarig et al., 2022). From 532 nm to 1064 nm, the lidar ratio increased by 36 %, which is in agreement with the previous observations at Leipzig (increase by 24–38 %; Haarig et al., 2022). The measured particle linear depolarization ratio of 20.6–25.0 % for the three different wavelengths indicates the presence of non-spherical particles, i.e., desert dust, but is somewhat smaller than what was typically observed for pure dust (Freudenthaler et al., 2009; Floutsi et al., 2023) indicating

200   the presence of some spherical non-dust particles. Considering the wavelength dependence of the particle linear depolarization ratio, a decrease of 18 % from 532 towards 1064 nm was observed. Similar findings were made at Leipzig and Morocco during SAMUM (decrease by 13–31 %; Freudenthaler et al., 2009; Haarig et al., 2022). The backscatter-related Ångström exponent in the lofted layer is on average around 0.31 for the wavelength pair 532/1064 nm, indicating large particles (i.e., desert dust).
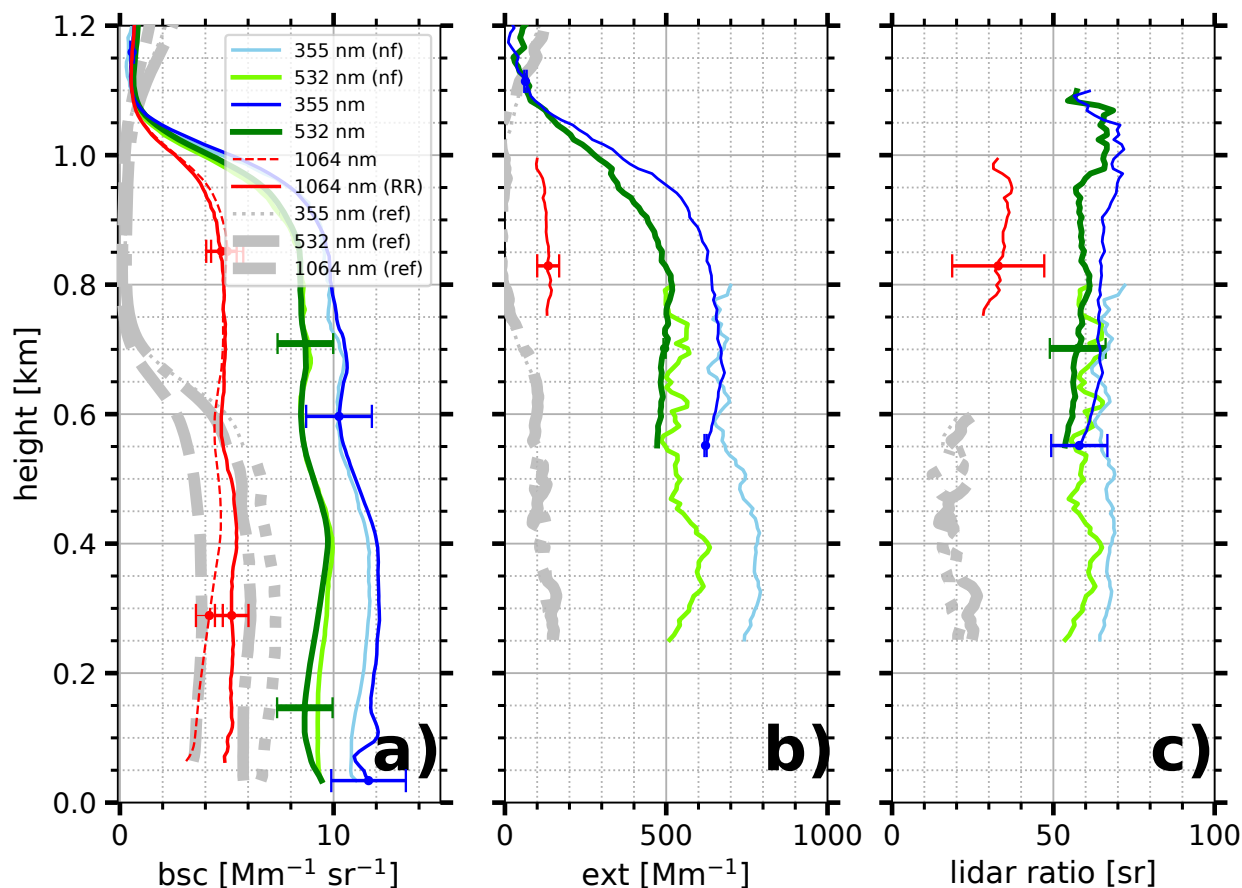
Figure 5. The same profiles as in Fig. 4 are shown here, but only for the PBL up to a height of 1.2 km. Furthermore, vertical smoothing was reduced to 67.5 m for the particle backscatter coefficient and to 187.5 m for the particle extinction coefficient and the lidar ratio at 355 and 532 nm and increased to 742.5 m for the particle extinction coefficient and the lidar ratio at 1064 nm. Near-field (nf) and far-field measurements are shown separately.

Considering the higher lidar ratio and the lower particle linear depolarization ratio on 24 September compared to the typical
205   values of pure desert dust we conclude that the dust on 24 September was slightly polluted.

    In contrast to the almost typical aerosol conditions in the lofted layer, an unusual strong pollution was observed in the PBL. The findings are highlighted in Fig. 5 showing zoomed profiles. In addition, vertical smoothing was reduced, which improves the accuracy of the near-field profiles. All mean values for the PBL are listed in Table 1 as well. On this day, extremely high values of the particle extinction coefficient were observed with layer mean values of 718, 547 and 126 Mm^{-1} (at 355, 532
210   and 1064 nm) between 0.25 and 1 km. The maximum values were even higher with 792, 635 and 145 Mm^{-1} (at 355, 532 and

Table 1. Layer mean values and standard deviation of the lidar-derived aerosol optical properties for the planetary boundary layer and the lofted layer on 24 September averaged from 04:38–05:57 UTC and on 16 September 2021 from 22:24–23:12 UTC. To avoid edge and overlap effects, the mean values were calculated for the following height ranges: lofted layer (ff measurements): 1.3–5.3 km (16 September with vertical smoothing as in Fig. 3) and 1.4–4.4 km (24 September with vertical smoothing as in Fig. 4); PBL (nf measurements): 0.06–0.6 km for backscatter-related properties and 0.25–0.6 km for extinction-related properties (16 September) and 0.06–1 km and 0.25–1 km, respectively (24 September), both with vertical smoothing as in Fig. 5.

Layer mean optical properties		PBL		lofted layer	
		24 Sep	16 Sep	24 Sep	16 Sep
		sulfate	marine	Saharan dust	
Particle backscatter coefficient [$Mm^{-1}sr^{-1}$]:	355 nm	10.4 ± 1.3	6.8 ± 0.5	1.9 ± 0.9	2.4 ± 0.5
	532 nm	8.7 ± 1.2	5.7 ± 0.4	2.4 ± 1.1	2.9 ± 0.6
	1064 nm	4.4 ± 0.5	3.6 ± 0.3	1.9 ± 0.9	1.8 ± 0.3
	1064 nm (RR)	4.9 ± 0.5	-	2.0 ± 0.8	-
Particle extinction coefficient [Mm^{-1}]:	355 nm	718 ± 51	114 ± 20	120 ± 64	138 ± 31
	532 nm	547 ± 38	130 ± 24	113 ± 65	134 ± 32
	1064 nm	126 ± 12	-	164 ± 23	-
Lidar ratio [sr]:	355 nm	66.7 ± 2.2	17.4 ± 2.5	65.3 ± 8.2	58.4 ± 1.3
	532 nm	60.1 ± 3.0	23.7 ± 6.8	50.7 ± 7.3	47.3 ± 2.2
	1064 nm	33.7 ± 2.3	-	68.7 ± 6.9	-
Particle linear depolarization ratio [%]:	355 nm	0.4 ± 0.3	0.7 ± 0.4	21.1 ± 2.2	24.5 ± 1.2
	532 nm	0.9 ± 0.5	1.1 ± 0.6	25.0 ± 1.5	28.1 ± 0.5
	1064 nm	1.2 ± 0.7	1.0 ± 0.5	20.6 ± 1.4	24.1 ± 0.9
Ångström exponent:	ext 355/532 nm	0.68 ± 0.13	−0.32 ± 0.61	0.10 ± 0.08	0.06 ± 0.08
	ext 532/1064 nm	1.63 ± 0.06	-	−0.10 ± 0.15	-
	bsc 355/532 nm	0.43 ± 0.06	0.41 ± 0.05	−0.46 ± 0.12	−0.47 ± 0.07
	bsc 532/1064 nm	0.96 ± 0.18	0.60 ± 0.04	0.31 ± 0.02	0.75 ± 0.06
	bsc 532/1064 nm (RR)	0.81 ± 0.04	-	0.24 ± 0.08	-
Aerosol optical depth:	355 nm	0.69 ± 0.08	0.08 ± 0.01	0.38 ± 0.25	0.57 ± 0.21
	532 nm	0.5 ± 0.08	0.08 ± 0.01	0.36 ± 0.24	0.57 ± 0.20

1064 nm). These values are 3–4 times higher than what was observed under clean marine conditions as shown for 16 September and indicated as grey lines in Fig. 5. Additionally, the particle extinction coefficient was strongly decreasing with increasing wavelength. A similar behavior was observed for the lidar ratio. Mean values of 66.7, 60.1 and 33.7 sr (at 355, 532 and 1064 nm)
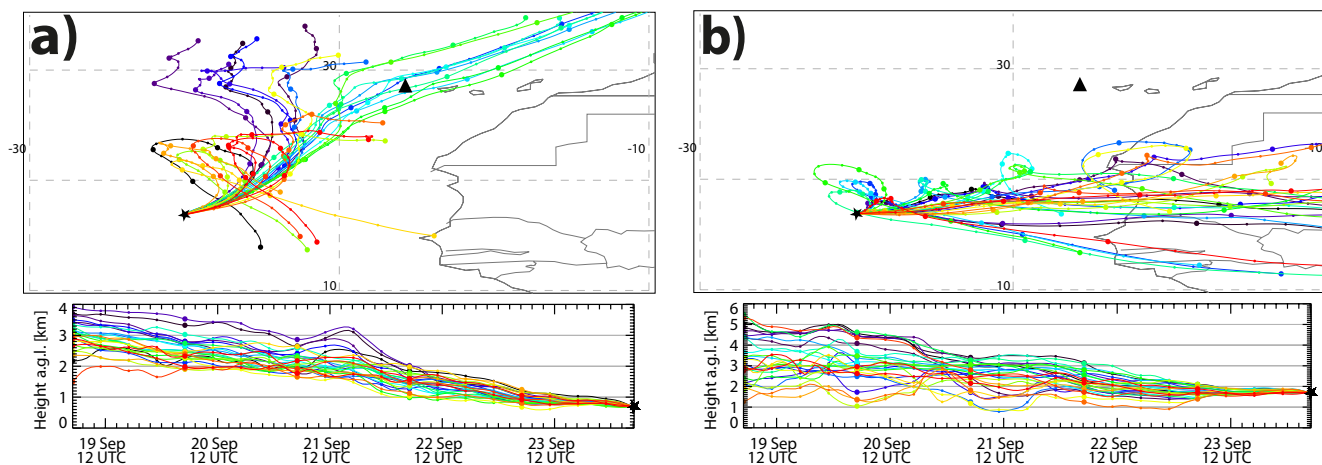
Figure 6. HYSPLIT ensemble trajectories for 120 hours back in time are shown. Air masses arriving at Mindelo (black star) on 24 September 2021, 5 UTC at (a) 0.7 km and (b) 1.7 km were computed. In the lower altitude they mainly originate from Las Palmas (black triangle), whereas in the higher altitude they were advected from the Sahara.

were found, showing a decrease by 44 % from 532 towards 1064 nm. The mean values of the lidar ratio are quite high compared

215 to the clean marine conditions and are typical for pollution or even smoke (Floutsi et al., 2023). However, the decrease of the lidar ratio at 1064 nm compared to the value at 532 nm points rather to pollution than to smoke. In the case of wildfire smoke an increase of the lidar ratio at 1064 nm was observed (Haarig et al., 2018). The high lidar ratio values point out the presence of particles, which are strongly attenuating the incoming solar radiation by scattering and absorption (Wandinger et al., 2023). The large extinction close to the ground indicates a strong pollution and explains the unusual high daily mean AOD of 1.1 and

220 0.9, which was measured with the sun photometer at 340 nm and 500 nm on this day. The lidar-derived total AOD between 04:38 and 05:57 UTC was 1.07 (355 nm) and 0.86 (532 nm) and, thus, in agreement with the values of the sun photometer measured during daytime. The AOD for the boundary layer only, as derived from the lidar measurements, was 0.69 at 355 nm and 0.5 at 532 nm and, thus, covered 58–64 % of the total lidar-derived AOD. Furthermore, visibility was strongly reduced on that day. Based on the maximum particle extinction coefficient at 532 nm, the visibility was around 6 km. The presence

225 of relatively small particles is further supported by the moderate wavelength dependence indicated by the backscatter-related Ångström exponent between 532 and 1064 nm (RR), which was 0.81 and the mean extinction-related Ångström exponent of only 0.68. The low values of the particle linear depolarization ratio of ≤ 1.1 % indicate that the observed particles are spherical.

4 Discussion

To summarize, both days – the 16 September 2021 (before the start of the eruption at Las Palmas) and the 24 September 2021

230 (during the volcanic episode) – had a similar aerosol layering structure with a planetary boundary layer ≤ 1 km and a lofted
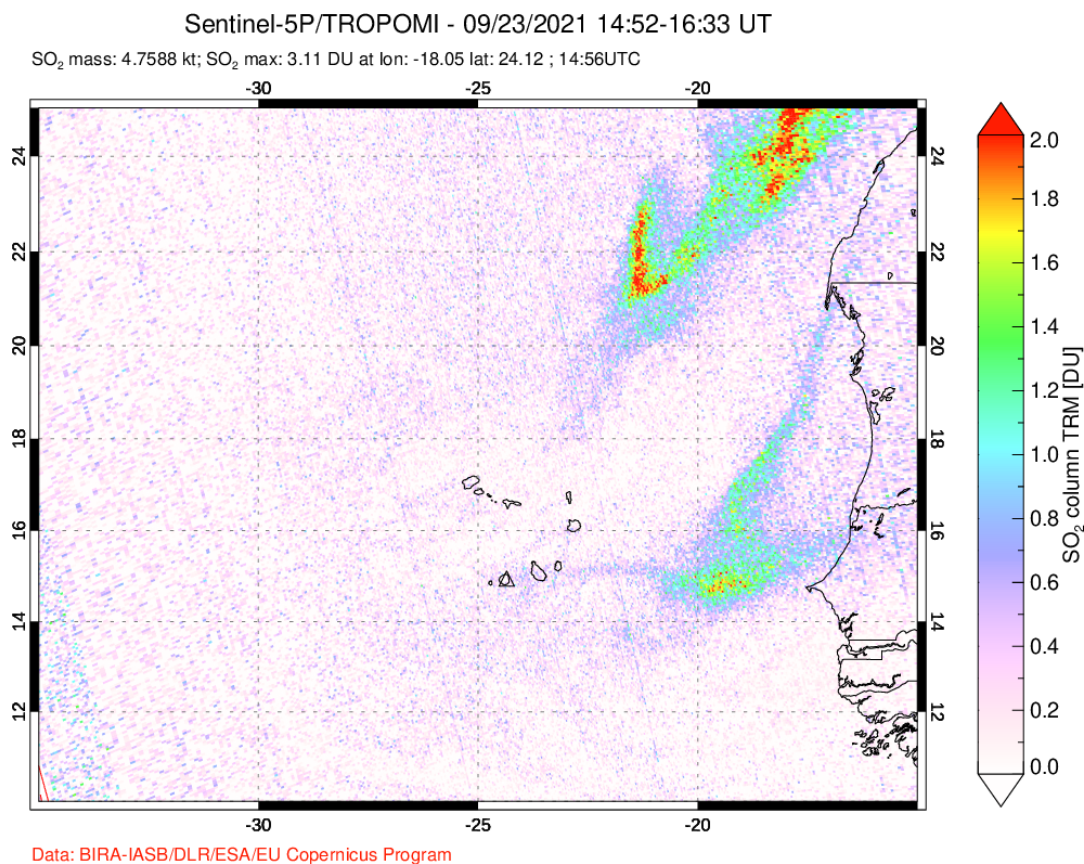
Figure 7. Satellite observations of TROPOMI on Sentinel-5P, which show the column integrated of SO_2 mass for the Cabo Verdean region on 23 September 2021 (TROPOMI, 2023).

layer of Saharan dust up to 6 km, typical for this time of the year at Cabo Verde. Both measurements were taken under similar meteorological conditions and, thus, well suitable to contrast the influence of the volcanic activity.

Although for the lofted layer, the lidar-derived aerosol optical properties slightly vary concerning the extent and intensity of the lofted layer between the 16 and 24 September 2021 with a lower layer top height, a lower particle linear depolarization

235 ratio and a higher lidar ratio on the 24 September, we can conclude that on both days the predominant aerosol type in the lofted layer was Saharan dust. Obviously, no volcanic ash was included in this layer on 24 September, because in that case we would have observed much higher values of the particle linear depolarization ratio (Groß et al., 2012). The higher lidar ratio observed on 24 September, however, indicate the presence of stronger absorbing particles slightly contaminating the SAL on that day. Considering the particle linear depolarization ratio and the lidar ratio together a contamination with continental

240 pollution or smoke is feasible. To corroborate the origin of the lofted aerosol layer on this day, 120 h HYSPLIT ensemble backward trajectories are shown in Fig. 6. Simulations of air mass arrival at Mindelo on 24 September, 5 UTC, at 0.7 km (Fig. 6a) and at 1.7 km (Fig. 6b) have been calculated. The trajectories for the higher altitude (Fig. 6b) show that the lofted

layer was influenced by an easterly flow, so that air masses were advected directly from the Saharan desert, which makes the occurrence and predominance of Saharan dust evident. However, partial mixing with sulfate during the transport over the
245 Atlantic Ocean cannot be ruled out as well as smoke and pollution contamination over the African continent. Fire spot analysis (FIRMS, firms.modaps.eosdis.nasa.gov, not shown) revealed only little fire activity along the transport path within the 120 h. Fires were detected at the eastern border of Algeria and close to the Mediterranean. Thus smoke contamination may have led to the light contamination of the SAL. However, we consider the presence of volcanic ash based on this analysis and the eruption mechanisms at Cumbre Vieja to be unlikely.

250 In contrast, the aerosol conditions in the PBL strongly differed between both analyzed measurement periods. While on 16 September, a clean marine PBL was present, a strong pollution was observed on 24 September with layer mean values of the particle extinction coefficient up to almost $800 \, \mathrm{Mm}^{-1}$, compared to $\leq 130 \, \mathrm{Mm}^{-1}$ during the clean marine conditions. The lidar ratio on that day was strongly enhanced as well with values around 60 sr compared to values for pure marine conditions of around 20 sr. The aerosol load in the PBL was furthermore responsible for 58–64 % of the total AOD in the analyzed time
255 period. In contrast, for the 16 September the contribution of the AOD in the PBL to the total AOD was only 12 %, i.e., more than 80 % of the total AOD was caused by the SAL. The observed pollution is associated to air masses coming from Las Palmas containing volcanic aerosol, which is supported by the HYSPLIT backward trajectories depicted in Fig. 6a. They illustrate a distinct advection of air masses from Canary Islands and, thus, from the volcano on Las Palmas. Additionally, FLEXPART simulations (Fig. C1) confirm these findings as they show air masses accumulating over the Atlantic Ocean on 18 September
260 before they pass from northwest over Las Palmas on 21 September and move further to Mindelo on 23 September. As the measured particle linear depolarization ratio is low in the PBL, the presence of ash particles can be excluded.

Instead, volcanic sulfate seems to be the dominating aerosol type in the PBL. It becomes more evident if the large amount of sulfur dioxide released by the volcano is taken into account. The SO_2 emissions were greatest at the beginning of the active period, reaching a maximum of 125 kt on 23 September 2021 (Milford et al., 2023). SO_2 was advected towards Mindelo as
265 can be seen in the satellite measurements of TROPOMI onboard Sentinel-5P (Fig. 7), showing the amount of SO_2 around the Cabo Verdean region during afternoon of 23 September 2021. The presence of SO_2 offered the possibility for secondary aerosol formation to sulfate particles, which is assumed to be the source of the observed particles. SO_2 quickly oxidates to sulfate aerosol with a high efficiency at warm temperatures and high relative humidity (Eatough et al., 1994; Yang et al., 2018). Favored conditions seem to be provided since the air masses are transported only over the Atlantic ocean in a tropic region.
270 According to Pattantyus et al. (2018), conversion rates are large $(3\text{–}50\,\%\,\mathrm{s}^{-1})$ especially in cloudy air, which is given as well due to the frequently occurring small clouds in the PBL as observed over the Cabo Verdean region.

In addition, not only SO_2 could have been advected from Las Palmas but also sulfate particles themselves. Filonchyk et al. (2022) identified, based on the single scattering albedo and the dissection of the AOD into a coarse and fine mode component, that on 24 September 2021 coarse-mode particles were almost absent at Las Palmas. Instead the presence of non-absorbing but
275 scattering fine-mode particles attributed to sulfate aerosol was shown, which could have been formed locally or were emitted directly by the volcano. As these observations are valid for a time period in which our case study was included, it strengthens our hypothesis, that we measured volcanic sulfate at Mindelo originating from Cumbre Vieja.

The presence of sulfate aerosol from the eruption at Las Palmas also becomes evident since the measured quantities are in agreement with previous lidar observations of volcanic sulfate. Furthermore, in this study it was the first time ever that

280   tropospheric volcanic sulfate was measured with a lidar at 1064 nm. During the eruption of Eyjafjallajökull in 2010, Navas-Guzmán et al. (2013) observed lofted aerosol layers between 1.5 and 3.5 km consisting to 82 % of fine-mode aerosol particles, i.e. sulfate particles over Granada, Spain. The corresponding values of the lidar ratio were 55 and 75 sr (355, 532 nm). Mona et al. (2012) recorded values of the lidar ratio up to 80 sr for volcanic sulfate from Eyjafjallajökull mixed with continental aerosol in the PBL over Potenza, Italy, while during the eruption of Mt. Etna in 2002 a lidar ratio of 55 ± 4 sr (355 nm) was

285   measured by Pappalardo et al. (2004) in a lofted aerosol layer of young sulfate particles mixed with a low amount of soot between 4 and 4.5 km over Potenza. With 66.7 and 60.1 sr (355, 532 nm) the observations over Mindelo on 24 September fit well into the range of values of the lidar ratio observed during the previous eruptions. Also the observed wavelength dependence with decreasing lidar ratio by 44 % from 532 towards 1064 nm confirms the assumptions in the CALIPSO aerosol typing which uses a lidar ratio of 50 sr at 532 nm and of 30 sr at 1064 nm for sulfate (Kim et al., 2018; Tackett et al., 2023). The particle linear

290   depolarization ratio measured on 24 September 2021 was with ≤ 1.1 % even smaller than the values observed for sulfate from Eyjafjallajökull, which was 4–5 % (Navas-Guzmán et al., 2013), indicating more clearly the presence of spherical (sulfate) particles. For the volcanic sulfate from Eyjafjallajökull, the backscatter-related Ångström exponent measured over Granada was 1.1 ± 0.2 for the the wavelength pair 355/532 and 2.1 ± 0.1 for 532/1064. During the measurement period, the values decreased to 0.7 ± 0.1 and 1.7 ± 0.3, respectively, due to hygroscopic growth of the sulfate particles. In a second layer of

295   volcanic sulfate, values of 1.7 ± 0.1 (355/532) and 1.4 ± 0.2 (532/1064) were observed, also decreasing significantly during the measurement period. Compared to these studies, the backscatter-related Ångström exponent measured over Mindelo on 24 September 2021 was smaller having values of only 0.43 ± 0.06 and 0.81 ± 0.04 (355/532, 532/1064 (RR)). These low values can be explained by hygroscopic growth of the sulfate particles since they were exposed to high humidity during their transport over the Atlantic ocean before they reached Mindelo. Furthermore, we expect that some marine particles were present in

300   the PBL above Mindelo, which are also spherical at high relative humidity (accounting to the low depolarization ratio). As marine particles are larger than the sulfate particles they reduced the backscatter-related Ångström exponent in contrast to the aforementioned observations whereat air masses were influenced by the European continent. The extinction-related Ångström exponent betwenn 355 and 532 nm observed over Mindelo was 0.68 ± 0.13 and, thus, closer to the previous observations at Granada whereat values of 0.7 ± 0.1 and 0.8 ± 0.1 were observed.

305   In this paper it is the first time ever that we can report the optical properties for the volcanic plume mixed in the marine PBL for all 3 (aerosol lidar) wavelengths by extending the observational capabilities towards 1064 nm. While the lidar ratios at 355 and 532 nm are in agreement with previous observations, the lidar ratio at 1064 nm of 33.7 sr and the extinction-related Ångström exponent of 1.6 have never been reported so far. Thus, it is a milestone for the characterization of volcanic sulfur with remote sensing techniques.

5 Summary and conclusions

In the frame of ESA's JATAC campaign to validate the Aeolus satellite, the multiwavelength-Raman-polarization lidar Polly^{XT} was installed at Mindelo, Cabo Verde, in June 2021 together with further instruments, e.g., an AERONET sun photometer. During the time of the campaign, a volcanic eruption at the Cumbre Vieja ridge at Las Palmas, Canary Islands, took place, starting on 19 September 2021. Volcanic activity was recorded until 13 December 2021. Due to the location of Mindelo in the

315 trade wind zone the preferred wind direction is northeast, i.e., from Canary Islands. Thus, advected air masses contaminated with volcanic aerosol were observed within the local PBL while the SAL above seemed little affected. The occurrence of volcanic aerosol at Mindelo was indicated by an increase of the columnar Ångström exponent and the AOD as measured by the sun photometer after 22 September 2021. Volcanic aerosol was furthermore observed with the Polly^{XT} lidar on multiple days during the whole time of volcanic activity. Exemplarily, a case study was shown for the 24 September 2021. On that day,

320 a pronounced pollution was seen over Cabo Verde, strongly contrasting the conditions observed before the start of the eruption. The intense pollution caused an unusually high AOD of more than 1.0 at different spectral bands. For a more detailed view, the vertically-resolved optical properties derived from the lidar were analyzed. They were compared to the lidar measurements from 16 September, which was before the start of the eruption and represents the typical aerosol conditions over Cabo Verde at this time of the year.

325 The lidar measurements for both days showed the presence of two distinct aerosol layers – the planetary boundary layer and a lofted layer of Saharan dust. For the 24 September, HYSPLIT trajectory calculations and FLEXPART simulations indicated a distinct advection of air masses from Las Palmas in the PBL. Air masses of the lofted layer originated from the Saharan desert. With the lidar, a strong pollution in the PBL was revealed. It led to an unusual high particle extinction coefficient of 718, 547 and 126 Mm^{-1} (mean values at 355, 532 and 1064 nm) and an enhanced lidar ratio of 66.7, 60.1 and 33.7 sr (mean values at

330 355, 532 and 1064 nm) in contrast to ≤ 130 Mm^{-1} and ≤ 23.7 sr within the clean marine PBL on the 16 September. Thus, on 24 September, the attenuation in the planetary boundary layer was increased by a factor of 3–4 compared to the background conditions. The visibility significantly decreased during these days down to 6 km. According to the measured particle extinction coefficient, the AOD for the planetary boundary layer was 0.69 at 355 nm and 0.5 at 532 nm. It accounts for 58-64 % of the total AOD. Compared to the AOD in the PBL of 0.08 (355 and 532 nm) during the clean marine PBL on 16 September 2021,

335 we can conclude that the pollution on 24 September accounted for 84–88 % of the AOD in the PBL on that day (AOD caused by pollution: 0.61 and 0.42 at 355 and 532 nm, respectively), i.e., only 12–16 % of the AOD in the PBL were caused by marine aerosol. Since the particle linear depolarization ratio in the PBL was close to 0 %, the presence of volcanic ash could be excluded. Instead, sulfate aerosol due to the volcanic eruption at Las Palmas seemed to be the dominating particle type in the low altitudes. This finding was furthermore supported by satellite measurements of Sentinel-5P, showing an advection of SO$_2$

340 towards Mindelo on 23 September, which was transformed to sulfate aerosol reaching Mindelo the day after.

In contrast, no indication for pure volcanic aerosol in the lofted layer could be found. The lidar ratio of 65.3, 50.7 and 68.7 sr were slightly higher compared to 58.4 and 47.3 sr (355, 532 nm) on 16 September 2021. Instead, the particle linear depolarization ratio of 21.1, 25.0 and 20.6 % (at 355, 532, 1064 nm) were lower than 24.5, 28.1 and 24.1 % (355, 532, 1064 nm),

which were observed on 16 September. However, Saharan dust as the major contributor can still be identified within this layer
345 (SAL) but probably slightly contaminated with smoke, pollution and/or sulfate.

While observations of Saharan dust have already been captured during several campaigns (e.g., SAMUM; Ansmann et al.,
2011a; Tesche et al., 2011), it was the first time that the optical properties of volcanic aerosol were observed at Cabo Verde with
a multiwavelength-Raman-polarization lidar. Lidar observations of volcanic ash exist for distinct eruptions like Eyjafjallajökull
(Ansmann et al., 2010; Groß et al., 2012) but lidar measurements of tropospheric volcanic sulfate aerosol, are very rare, yet.
350 One additional benefit of this study is the first ever availability of measurements of the particle extinction coefficient and the
lidar ratio at 1064 nm for this aerosol type. Having measurements at all three wavelengths allows us to get new insights in
lidar-based aerosol typing and to enlarge our data sets. The findings of this study provide useful insights on the lidar-derived
optical properties of volcanic aerosol. They can in turn be used to further improve the aerosol typing by multiwavelength-
Raman-polarization lidars, as well as space-borne lidars as NASA's CALIOP or ESA's Aeolus and EarthCARE, or assist in the
355 development of new aerosol typing schemes. As the focus of the campaign at Cabo Verde was on the Aeolus Cal/Val activities,
there is also the possibility for further research on the potential of Aeolus to capture the volcanic plume on its way to Cabo
Verde, which is planned for future studies. Finally, the observation of this event highlights the necessity for ground-based lidar
stations in remote areas. With respect to that, a permanent station within the framework of ACTRIS is foreseen in Mindelo.

Data availability. The Polly[XT] lidar data will be made available via ACTRIS services. Near-real-time measurement quicklooks can be found
360 at https://polly.tropos.de/. AERONET data was downloaded from https://aeronet.gsfc.nasa.gov/cgi-bin/data_display_aod_v3?site=Mindelo_
OSCM&nachal=0&year=2021&month=9&day=24&aero_water=0&level=3&if_day=0&if_err=0&place_code=10&year_or_month=0/, last
access: 9 March 2023. HYSPLIT trajectories were calculated using the online tool on https://www.ready.noaa.gov/hypub-bin/trajtype.pl?
runtype=archive with meteorological input data from GDAS1 (https://www.ready.noaa.gov/gdas1.php), last access: 20 January 2023. The
data for the FLEXPART analysis was taken from https://doi.org/10.5065/D6M043C6, last access: 24 September 2021. The TROPOMI SO_2
365 plot is taken from https://so2.gsfc.nasa.gov/pix/daily/ixxxza/troploop5pca.php?yr=21&mo=09&dy=23&bn=cverde. The underlying data was
downloaded from the S5P-PAL data portal (https://data-portal.s5p-pal.com/) from July 2022 onward, and from BIRA-IASB distributions
website (https://distributions.aeronomie.be/) for older data, last access: 13 March 2023.

Appendix A: AOD and lidar profiles
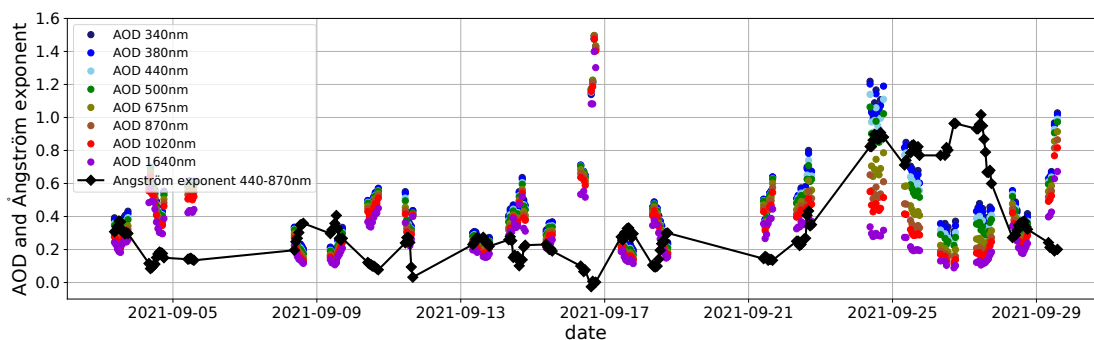
Figure A1. Same as Figure 1 but including the measurement of 16 September 2021 which was contaminated by a cirrus cloud.
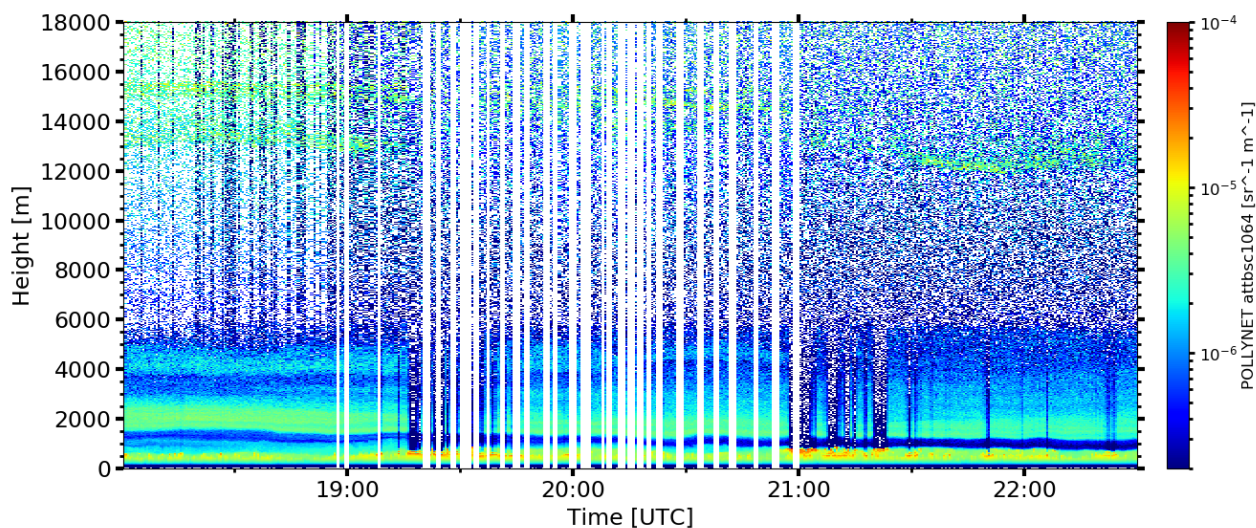
Figure A2. Temporal evolution of the attenuated backscatter coefficient at 1064 nm measured by Polly^{XT} at Mindelo, Cabo Verde, during 16 September 2021, 18–22:30 UTC. In an altitude between 12 and 16 km the Cirrus cloud located, which was not correctly screened out by the AERONET algorithm.

Appendix B: Flexpart simulations
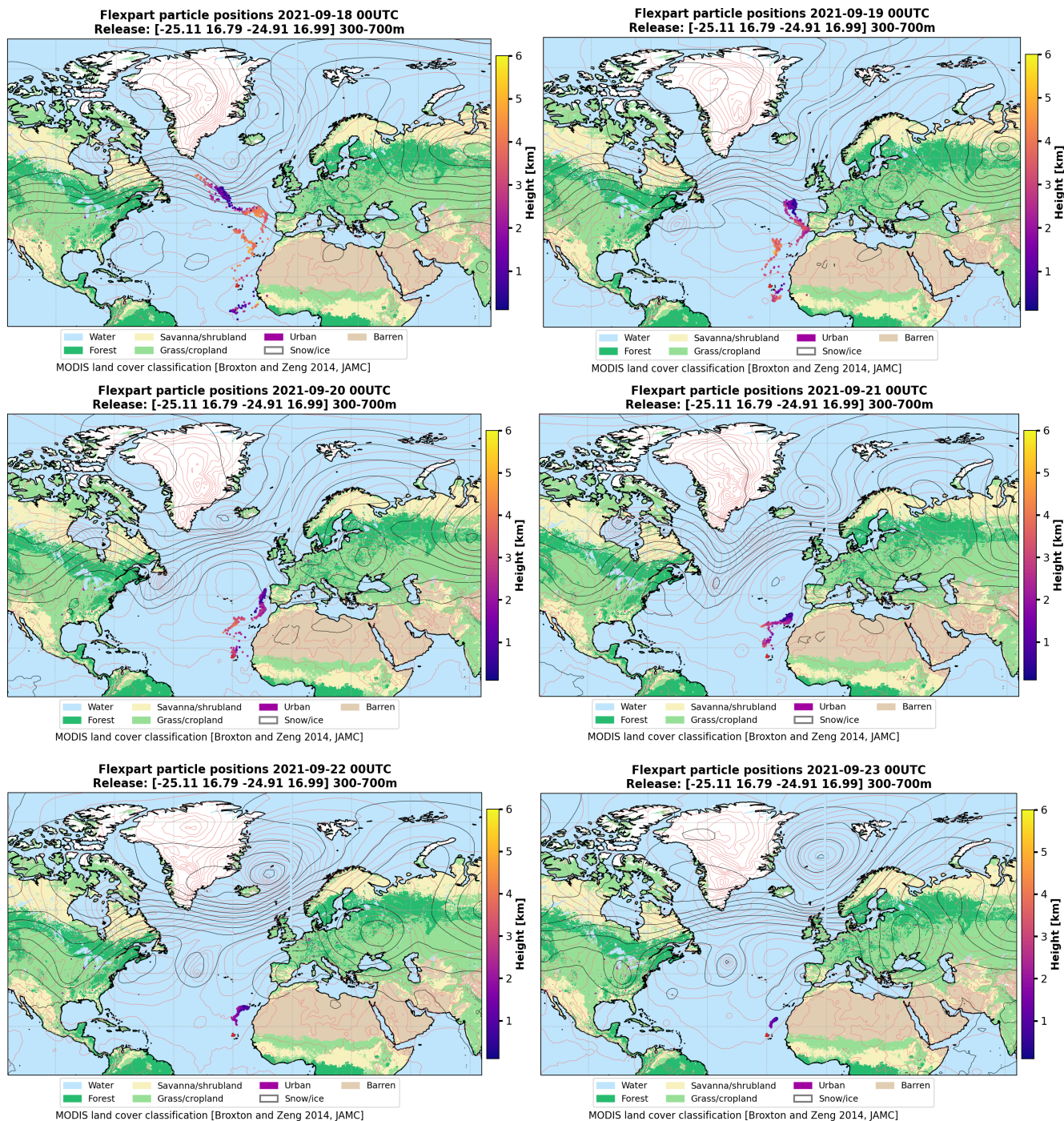
Figure C1. Selected Flexpart simulations show the location of single air parcels between 18 and 23 September 2021, each at 0 UTC, before they arrive at Mindelo (red triangle) at 500 m on 24 September 2021, 6 UTC. The colour of the dots indicates their heigh above ground. MODIS land cover classification according to Broxton et al. (2014).

370 *Author contributions.* HG conceptualized the manuscript together with HB and AAF. MH provided the data of the lidar extinction measurements at 1064 nm. MR performed the FLEXPART simulations. AA contributed his expertise on lidar data analysis and volcanic aerosol. RE, DA, HB, and AS have been responsible for the deployment and operation of the ground-based instruments at Mindelo. CZ coordinates the scientific activities at OSCM, Cabo Verde. All coauthors were actively involved in the extended discussions and the elaboration of the final design of the manuscript.

375 *Competing interests.* The authors declare that they have no conflict of interest.

Acknowledgements. This research has been supported by the German Federal Ministry for Economic Affairs and Energy (BMWi) (grant no. 50EE1721C) and Horizon 2020 (grant nos. 654109 and 7395302). We furthermore acknowledge gratefully the team of OSCM for their support without which it would not have been possible to perform the observations. We also would like to thank ESA and the ASKOS/JATAC teams for the organization of the campaign and the support during the whole time!

References

AERONET(2023): Aerosol Robotic Network, available at https://aeronet.gsfc.nasa.gov/cgi-bin/data_display_aod_v3?site=Mindelo_ OSCM&nachal=0&year=2021&month=9&day=24&aero_water=0&level=3&if_day=0&if_err=0&place_code=10&year_or_month=0/, last access: 9 March, 2023.

Aiuppa, A., Giudice, G., Gurrieri, S., Liuzzo, M., Burton, M., Caltabiano, T., McGonigle, A. J. S., Salerno, G., Shinohara, H., and Valenza, M.: Total volatile flux from Mount Etna, Geophysical Research Letters, 35, https://doi.org/10.1029/2008GL035871, 2008.

Althausen, D., Engelmann, R., Baars, H., Heese, B., Ansmann, A., Müller, D., and Komppula, M.: Portable Raman Lidar PollyXT for Automated Profiling of Aerosol Backscatter, Extinction, and Depolarization, Journal of Atmospheric and Oceanic Technology, 26, 2366 – 2378, https://doi.org/10.1175/2009JTECHA1304.1, 2009.

Amiridis, V., Kampouri, A., Gkikas, A., Misios, S., Gialitaki, A., Marinou, E., Rennie, M., Benedetti, A., Solomos, S., Zanis, P., et al.: Aeolus winds impact on volcanic ash early warning systems for aviation, Scientific Reports, 13, 1–14, https://doi.org/10.1038/s41598-023-34715-6, 2023.

Amiridis, V. et al.: The ASKOS experiment for desert dust science applications, EGU General Assembly 2022, Vienna, Austria, 23–27 May 2022, EGU22-3633, Tech. rep., Copernicus Meetings, https://doi.org/10.5194/egusphere-egu22-3633, 2022.

Ansmann, A., Wandinger, U., Riebesell, M., Weitkamp, C., and Michaelis, W.: Independent measurement of extinction and backscatter profiles in cirrus clouds by using a combined Raman elastic-backscatter lidar, Appl. Opt., 31, 7113–7131, https://doi.org/10.1364/AO.31.007113, 1992.

Ansmann, A., Tesche, M., Groß, S., Freudenthaler, V., Seifert, P., Hiebsch, A., Schmidt, J., Wandinger, U., Mattis, I., Müller, D., and Wiegner, M.: The 16 April 2010 major volcanic ash plume over central Europe: EARLINET lidar and AERONET photometer observations at Leipzig and Munich, Germany, Geophysical Research Letters, 37, https://doi.org/10.1029/2010GL043809, 2010.

Ansmann, A., Petzold, A., Kandler, K., Tegen, I., Wendisch, M., Mueller, D., Weinzierl, B., Mueller, T., and Heintzenberg, J.: Saharan Mineral Dust Experiments SAMUM–1 and SAMUM–2: what have we learned?, Tellus B: Chemical and Physical Meteorology, 63, 403–429, https://doi.org/10.1111/j.1600-0889.2011.00555.x, 2011a.

Ansmann, A., Tesche, M., Seifert, P., Groß, S., Freudenthaler, V., Apituley, A., Wilson, K. M., Serikov, I., Linné, H., Heinold, B., Hiebsch, A., Schnell, F., Schmidt, J., Mattis, I., Wandinger, U., and Wiegner, M.: Ash and fine-mode particle mass profiles from EARLINET-AERONET observations over central Europe after the eruptions of the Eyjafjallajökull volcano in 2010, Journal of Geophysical Research: Atmospheres, 116, https://doi.org/10.1029/2010JD015567, 2011b.

Baars, H., Kanitz, T., Engelmann, R., Althausen, D., Heese, B., Komppula, M., Preißler, J., Tesche, M., Ansmann, A., Wandinger, U., et al.: An overview of the first decade of PollyNET: an emerging network of automated Raman-polarization lidars for continuous aerosol profiling, https://doi.org/10.5194/acp-16-5111-2016, 2016.

Bohlmann, S., Baars, H., Radenz, M., Engelmann, R., and Macke, A.: Ship-borne aerosol profiling with lidar over the Atlantic Ocean: from pure marine conditions to complex dust–smoke mixtures, Atmospheric Chemistry and Physics, 18, 9661–9679, https://doi.org/10.5194/acp-18-9661-2018, 2018.

Broxton, P. D., Zeng, X., Sulla-Menashe, D., and Troch, P. A.: A Global Land Cover Climatology Using MODIS Data, Journal of Applied Meteorology and Climatology, 53, 1593 – 1605, https://doi.org/10.1175/JAMC-D-13-0270.1, 2014.

415 Businger, S., Huff, R., Pattantyus, A., Horton, K., Sutton, A. J., Elias, T., and Cherubini, T.: Observing and Forecasting Vog Dispersion from Kīlauea Volcano, Hawaii, Bulletin of the American Meteorological Society, 96, 1667 – 1686, https://doi.org/10.1175/BAMS-D-14-00150.1, 2015.

Carracedo, J. C., Troll, V. R., Day, J. M. D., Geiger, H., Aulinas, M., Soler, V., Deegan, F. M., Perez-Torrado, F. J., Gisbert, G., Gazel, E., Rodriguez-Gonzalez, A., and Albert, H.: The 2021 eruption of the Cumbre Vieja volcanic ridge on La Palma, Canary Islands, Geology
420 Today, 38, 94–107, https://doi.org/10.1111/gto.12388, 2022.

Deshler, T.: A review of global stratospheric aerosol: Measurements, importance, life cycle, and local stratospheric aerosol, Atmospheric Research, 90, 223–232, https://doi.org/10.1016/j.atmosres.2008.03.016, 17th International Conference on Nucleation and Atmospheric Aerosols, 2008.

Eatough, D., Caka, F., and Farber, R.: The Conversion of SO2 to Sulfate in the Atmosphere, Israel Journal of Chemistry, 34, 301–314,
425 https://doi.org/10.1002/ijch.199400034, 1994.

Engelmann, R., Kanitz, T., Baars, H., Heese, B., Althausen, D., Skupin, A., Wandinger, U., Komppula, M., Stachlewska, I. S., Amiridis, V., Marinou, E., Mattis, I., Linné, H., and Ansmann, A.: The automated multiwavelength Raman polarization and water-vapor lidar Polly^{XT}: the neXT generation, Atmospheric Measurement Techniques, 9, 1767–1784, https://doi.org/10.5194/amt-9-1767-2016, 2016.

Fehr, T., McCarthy, W., Amiridis, V., Baars, H., von Bismarck, J., Borne, M., Chen, S., Flamant, C., Marenco, F., Knipperz, P., et al.: The
430 Joint Aeolus Tropical Atlantic Campaign 2021/2022 Overview–Atmospheric Science and Satellite Validation in the Tropics, EGU General Assembly 2023, Vienna, Austria, 24–28 Apr 2023, EGU23-7249, Tech. rep., https://doi.org/10.5194/egusphere-egu23-7249, 2023.

Filonchyk, M., Peterson, M. P., Gusev, A., Hu, F., Yan, H., and Zhou, L.: Measuring air pollution from the 2021 Canary Islands volcanic eruption, Science of The Total Environment, 849, 157 827, https://doi.org/10.1016/j.scitotenv.2022.157827, 2022.

Floutsi, A. A., Baars, H., Engelmann, R., Althausen, D., Ansmann, A., Bohlmann, S., Heese, B., Hofer, J., Kanitz, T., Haarig, M., Ohneiser,
435 K., Radenz, M., Seifert, P., Skupin, A., Yin, Z., Abdullaev, S. F., Komppula, M., Filioglou, M., Giannakaki, E., Stachlewska, I. S., Janicka, L., Bortoli, D., Marinou, E., Amiridis, V., Gialitaki, A., Mamouri, R.-E., Barja, B., and Wandinger, U.: DeLiAn – a growing collection of depolarization ratio, lidar ratio and Ångström exponent for different aerosol types and mixtures from ground-based lidar observations, Atmospheric Measurement Techniques, 16, 2353–2379, https://doi.org/10.5194/amt-16-2353-2023, 2023.

Freudenthaler, V., Esselborn, M., Wiegner, M., Heese, B., Tesche, M., Ansmann, A., Müller, D., Althausen, D., Wirth, M., Fix, A., Ehret, G.,
440 Knippertz, P., Toledano, C., Gasteiger, J., Garhammer, M., and Seefeldner, M.: Depolarization ratio profiling at several wavelengths in pure Saharan dust during SAMUM 2006, Tellus B: Chemical and Physical Meteorology, https://doi.org/10.1111/j.1600-0889.2008.00396.x, 2009.

GDAS1(2023): Global Data and Assimilation Service, meteorological data, information available at: https://www.ready.noaa.gov/gdas1.php, last access: 20 January, 2023.

445 Groß, S., Tesche, M., Freudenthaler, V., Toledano, C., Wiegner, M., Ansmann, A., Althausen, D., and Seefeldner, M.: Characterization of Saharan dust, marine aerosols and mixtures of biomass-burning aerosols and dust by means of multi-wavelength depolarization and Raman lidar measurements during SAMUM 2, Tellus B: Chemical and Physical Meteorology, 63, 706–724, https://doi.org/10.1111/j.1600-0889.2011.00556.x, 2011.

Groß, S., Freudenthaler, V., Wiegner, M., Gasteiger, J., Geiß, A., and Schnell, F.: Dual-wavelength linear depolarization ratio of vol-
450 canic aerosols: Lidar measurements of the Eyjafjallajökull plume over Maisach, Germany, Atmospheric Environment, 48, 85–96, https://doi.org/10.1016/j.atmosenv.2011.06.017, volcanic ash over Europe during the eruption of Eyjafjallajöekull on Iceland, April-May 2010, 2012.

Haarig, M., Engelmann, R., Ansmann, A., Veselovskii, I., Whiteman, D. N., and Althausen, D.: 1064 nm rotational Raman lidar for particle extinction and lidar-ratio profiling: cirrus case study, Atmospheric Measurement Techniques, 9, 4269–4278, https://doi.org/10.5194/amt-9-4269-2016, 2016.

Haarig, M., Ansmann, A., Althausen, D., Klepel, A., Groß, S., Freudenthaler, V., Toledano, C., Mamouri, R.-E., Farrell, D. A., Prescod, D. A., Marinou, E., Burton, S. P., Gasteiger, J., Engelmann, R., and Baars, H.: Triple-wavelength depolarization-ratio profiling of Saharan dust over Barbados during SALTRACE in 2013 and 2014, Atmospheric Chemistry and Physics, 17, 10767–10794, https://doi.org/10.5194/acp-17-10767-2017, 2017.

Haarig, M., Ansmann, A., Baars, H., Jimenez, C., Veselovskii, I., Engelmann, R., and Althausen, D.: Depolarization and lidar ratios at 355, 532, and 1064 nm and microphysical properties of aged tropospheric and stratospheric Canadian wildfire smoke, Atmospheric Chemistry and Physics, 18, 11847–11861, https://doi.org/10.5194/acp-18-11847-2018, 2018.

Haarig, M., Ansmann, A., Engelmann, R., Baars, H., Toledano, C., Torres, B., Althausen, D., Radenz, M., and Wandinger, U.: First triple-wavelength lidar observations of depolarization and extinction-to-backscatter ratios of Saharan dust, Atmospheric Chemistry and Physics, 22, 355–369, https://doi.org/10.5194/acp-22-355-2022, 2022.

Hansen, J., Sato, M., Lacis, A., and Ruedy, R.: The missing climate forcing, Philosophical Transactions of the Royal Society of London. Series B: Biological Sciences, 352, 231–240, https://doi.org/10.1098/rstb.1997.0018, 1997.

Holben, B., Eck, T., Slutsker, I., Tanré, D., Buis, J., Setzer, A., Vermote, E., Reagan, J., Kaufman, Y., Nakajima, T., Lavenu, F., Jankowiak, I., and Smirnov, A.: AERONET—A Federated Instrument Network and Data Archive for Aerosol Characterization, Remote Sensing of Environment, 66, 1–16, https://doi.org/10.1016/S0034-4257(98)00031-5, 1998.

HYSPLIT(2023): HYbrid Single-Particle Lagrangian Integrated Trajectory model, backward trajectory calculation tool, available at: http://ready.arl.noaa.gov/HYSPLIT_traj.php, last access: 20 January, 2023.

Jimenez, C., Ansmann, A., Engelmann, R., Donovan, D., Malinka, A., Seifert, P., Wiesen, R., Radenz, M., Yin, Z., Bühl, J., Schmidt, J., Barja, B., and Wandinger, U.: The dual-field-of-view polarization lidar technique: a new concept in monitoring aerosol effects in liquid-water clouds – case studies, Atmospheric Chemistry and Physics, 20, 15265–15284, https://doi.org/10.5194/acp-20-15265-2020, 2020.

John, W. et al.: Size distribution characteristics of aerosols, vol. 3, pp. 41–54, John Wiley & Sons, Inc., Hoboken, NJ, USA, 2011.

Jäger, H.: Long-term record of lidar observations of the stratospheric aerosol layer at Garmisch-Partenkirchen, Journal of Geophysical Research: Atmospheres, 110, https://doi.org/10.1029/2004JD005506, 2005.

Kampouri, A., Amiridis, V., Solomos, S., Gialitaki, A., Marinou, E., Spyrou, C., Georgoulias, A. K., Akritidis, D., Papagiannopoulos, N., Mona, L., Scollo, S., Tsichla, M., Tsikoudi, I., Pytharoulis, I., Karacostas, T., and Zanis, P.: Investigation of Volcanic Emissions in the Mediterranean: "The Etna–Antikythera Connection", Atmosphere, 12, https://doi.org/10.3390/atmos12010040, 2021.

Kim, M.-H., Omar, A. H., Tackett, J. L., Vaughan, M. A., Winker, D. M., Trepte, C. R., Hu, Y., Liu, Z., Poole, L. R., Pitts, M. C., Kar, J., and Magill, B. E.: The CALIPSO version 4 automated aerosol classification and lidar ratio selection algorithm, Atmospheric Measurement Techniques, 11, 6107–6135, https://doi.org/10.5194/amt-11-6107-2018, 2018.

Marinou, E., Paschou, P., Tsikoudi, I., Tsekeri, A., Daskalopoulou, V., Kouklaki, D., Siomos, N., Spanakis-Misirlis, V., Voudouri, K. A., Georgiou, T., Drakaki, E., Kampouri, A., Papachristopoulou, K., Mavropoulou, I., Mallios, S., Proestakis, E., Gkikas, A., Koutsoupi, I., Raptis, I. P., Kazadzis, S., Baars, H., Floutsi, A., Pirloaga, R., Nemuc, A., Marenco, F., Kezoudi, M., Papetta, A., Močnik, G., Díez, J. Y., Ryder, C. L., Ratcliffe, N., Kandler, K., Sudharaj, A., and Amiridis, V.: An Overview of the ASKOS Campaign in Cabo Verde, Environmental Sciences Proceedings, 26, https://doi.org/10.3390/environsciproc2023026200, 2023.

490   Martin, E., Bekki, S., Ninin, C., and Bindeman, I.: Volcanic sulfate aerosol formation in the troposphere, Journal of Geophysical Research: Atmospheres, 119, 12,660–12,673, https://doi.org/10.1002/2014JD021915, 2014.

McGonigle, A. J. S., Delmelle, P., Oppenheimer, C., Tsanev, V. I., Delfosse, T., Williams-Jones, G., Horton, K., and Mather, T. A.: SO2 depletion in tropospheric volcanic plumes, Geophysical Research Letters, 31, https://doi.org/10.1029/2004GL019990, 2004.

Miffre, A., David, G., Thomas, B., Rairoux, P., Fjaeraa, A., Kristiansen, N., and Stohl, A.: Volcanic aerosol optical properties and
495   phase partitioning behavior after long-range advection characterized by UV-Lidar measurements, Atmospheric Environment, 48, 76–84, https://doi.org/10.1016/j.atmosenv.2011.03.057, volcanic ash over Europe during the eruption of Eyjafjallajöekull on Iceland, April-May 2010, 2012.

Milford, C., Torres, C., Vilches, J., Gossman, A.-K., Weis, F., Suárez-Molina, D., García, O. E., Prats, N., Barreto, Á., García, R. D., et al.: Impact of the 2021 La Palma volcanic eruption on air quality: Insights from a multidisciplinary approach, Science of the Total
500   Environment, 869, 161 652, https://doi.org/10.1016/j.scitotenv.2023.161652, 2023.

Mona, L., Amodeo, A., D'Amico, G., Giunta, A., Madonna, F., and Pappalardo, G.: Multi-wavelength Raman lidar observations of the Eyjaf-jallajökull volcanic cloud over Potenza, southern Italy, Atmospheric Chemistry and Physics, 12, 2229–2244, https://doi.org/10.5194/acp-12-2229-2012, 2012.

National Centers for Environmental Prediction, National Weather Service, NOAA, U.S. Department of Commerce: NCEP FNL Operational
505   Model Global Tropospheric Analyses, continuing from July 1999, https://doi.org/10.5065/D6M043C6, 2000.

Navas-Guzmán, F., Müller, D., Bravo-Aranda, J. A., Guerrero-Rascado, J. L., Granados-Muñoz, M. J., Pérez-Ramírez, D., Olmo, F. J., and Alados-Arboledas, L.: Eruption of the Eyjafjallajökull Volcano in spring 2010: Multiwavelength Raman lidar measurements of sulphate particles in the lower troposphere, Journal of Geophysical Research: Atmospheres, 118, 1804–1813, https://doi.org/10.1002/jgrd.50116, 2013.

510   Pappalardo, G., Amodeo, A., Mona, L., Pandolfi, M., Pergola, N., and Cuomo, V.: Raman lidar observations of aerosol emitted during the 2002 Etna eruption, Geophysical Research Letters, 31, https://doi.org/10.1029/2003GL019073, 2004.

Pappalardo, G., Mona, L., D'Amico, G., Wandinger, U., Adam, M., Amodeo, A., Ansmann, A., Apituley, A., Alados Arboledas, L., Balis, D., Boselli, A., Bravo-Aranda, J. A., Chaikovsky, A., Comeron, A., Cuesta, J., De Tomasi, F., Freudenthaler, V., Gausa, M., Giannakaki, E., Giehl, H., Giunta, A., Grigorov, I., Groß, S., Haeffelin, M., Hiebsch, A., Iarlori, M., Lange, D., Linné, H., Madonna, F., Mattis, I.,
515   Mamouri, R.-E., McAuliffe, M. A. P., Mitev, V., Molero, F., Navas-Guzman, F., Nicolae, D., Papayannis, A., Perrone, M. R., Pietras, C., Pietruczuk, A., Pisani, G., Preißler, J., Pujadas, M., Rizi, V., Ruth, A. A., Schmidt, J., Schnell, F., Seifert, P., Serikov, I., Sicard, M., Simeonov, V., Spinelli, N., Stebel, K., Tesche, M., Trickl, T., Wang, X., Wagner, F., Wiegner, M., and Wilson, K. M.: Four-dimensional distribution of the 2010 Eyjafjallajökull volcanic cloud over Europe observed by EARLINET, Atmospheric Chemistry and Physics, 13, 4429–4450, https://doi.org/10.5194/acp-13-4429-2013, 2013.

520   Pattantyus, A. K., Businger, S., and Howell, S. G.: Review of sulfur dioxide to sulfate aerosol chemistry at Kīlauea Volcano, Hawai'i, Atmospheric Environment, 185, 262–271, https://doi.org/10.1016/j.atmosenv.2018.04.055, 2018.

Radenz, M., Seifert, P., Baars, H., Floutsi, A. A., Yin, Z., and Bühl, J.: Automated time–height-resolved air mass source attribution for profiling remote sensing applications, Atmospheric Chemistry and Physics, 21, 3015–3033, https://doi.org/10.5194/acp-21-3015-2021, 2021.

525   Rittmeister, F., Ansmann, A., Engelmann, R., Skupin, A., Baars, H., Kanitz, T., and Kinne, S.: Profiling of Saharan dust from the Caribbean to western Africa – Part 1: Layering structures and optical properties from shipborne polarization/Raman lidar observations, Atmospheric Chemistry and Physics, 17, 12 963–12 983, https://doi.org/10.5194/acp-17-12963-2017, 2017.

Robock, A.: Volcanic eruptions and climate, Reviews of Geophysics, 38, 191–219, https://doi.org/10.1029/1998RG000054, 2000.

Rolph, G., Stein, A., and Stunder, B.: Real-time Environmental Applications and Display sYstem: READY, Environmental Modelling &
530   Software, 95, 210–228, https://doi.org/10.1016/j.envsoft.2017.06.025, 2017.

Solomon, S., Daniel, J. S., Neely, R. R., Vernier, J.-P., Dutton, E. G., and Thomason, L. W.: The Persistently Variable "Background" Strato-
    spheric Aerosol Layer and Global Climate Change, Science, 333, 866–870, https://doi.org/10.1126/science.1206027, 2011.

Stein, A. F., Draxler, R. R., Rolph, G. D., Stunder, B. J. B., Cohen, M. D., and Ngan, F.: NOAA's HYSPLIT Atmospheric Transport and
    Dispersion Modeling System, Bulletin of the American Meteorological Society, 96, 2059–2077, https://doi.org/10.1175/BAMS-D-14-
535   00110.1, 2015.

Tackett, J. L., Kar, J., Vaughan, M. A., Getzewich, B. J., Kim, M.-H., Vernier, J.-P., Omar, A. H., Magill, B. E., Pitts, M. C., and Winker,
    D. M.: The CALIPSO version 4.5 stratospheric aerosol subtyping algorithm, Atmospheric Measurement Techniques, 16, 745–768,
    https://doi.org/10.5194/amt-16-745-2023, 2023.

Tesche, M., Gross, S., Ansmann, A., Mueller, D., Althausen, D., Freudenthaler, V., and Esselborn, M.: Profiling of Saharan dust and biomass-
540   burning smoke with multiwavelength polarization Raman lidar at Cape Verde, Tellus B: Chemical and Physical Meteorology, 63, 649–676,
    https://doi.org/10.1111/j.1600-0889.2011.00548.x, 2011.

TROPOMI(2023): TROPOspheric Monitoring Instrument, quicklooks available at https://so2.gsfc.nasa.gov/pix/daily/ixxxza/troploop5pca.
    php?yr=21&mo=09&dy=23&bn=cverde, unerlaying data available at https://data-portal.s5p-pal.com/) from July 2022 onward and at
    https://distributions.aeronomie.be/for older data, last access: 13 March 2023, 2023.

545 Veefkind, J., Aben, I., McMullan, K., Förster, H., de Vries, J., Otter, G., Claas, J., Eskes, H., de Haan, J., Kleipool, Q., van Weele, M.,
    Hasekamp, O., Hoogeveen, R., Landgraf, J., Snel, R., Tol, P., Ingmann, P., Voors, R., Kruizinga, B., Vink, R., Visser, H., and Levelt, P.:
    TROPOMI on the ESA Sentinel-5 Precursor: A GMES mission for global observations of the atmospheric composition for climate, air
    quality and ozone layer applications, Remote Sensing of Environment, 120, 70–83, https://doi.org/10.1016/j.rse.2011.09.027, the Sentinel
    Missions - New Opportunities for Science, 2012.

550 Wandinger, U., Floutsi, A. A., Baars, H., Haarig, M., Ansmann, A., Hünerbein, A., Docter, N., Donovan, D., van Zadelhoff, G.-J., Mason, S.,
    and Cole, J.: HETEAC – the Hybrid End-To-End Aerosol Classification model for EarthCARE, Atmospheric Measurement Techniques,
    16, 2485–2510, https://doi.org/10.5194/amt-16-2485-2023, 2023.

Yang, S., Ma, Y., Duan, F., He, K., Wang, L., Wei, Z., Zhu, L., Ma, T., Li, H., and Ye, S.: Characteristics and formation of typ-
    ical winter haze in Handan, one of the most polluted cities in China, Science of The Total Environment, 613-614, 1367–1375,
555   https://doi.org/10.1016/j.scitotenv.2017.08.033, 2018.

Yin, Z. and Baars, H.: PollyNET/Pollynet_Processing_Chain: Version 3.0, https://doi.org/10.5281/zenodo.5571289, 2021.

Zhang, Y., Zhu, X., Slanina, S., Shao, M., Zeng, L., Hu, M., Bergin, M., and Salmon, L.: Aerosol pollution in some Chinese cities (IUPAC
    Technical Report), Pure and Applied Chemistry, 76, 1227–1239, https://doi.org/10.1351/pac200476061227, 2004.